Microelectronics Reliability 169 (2025) 115754

Contents lists available at ScienceDirect

Microelectronics Reliability

journal homepage: www.elsevier.com/locate/microrel

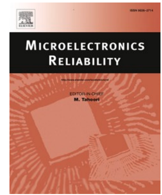

Research paper

Micro-Raman and SEM analyses of failed GaN HEMT multilayer architecture

Enza Fazio [a], Cettina Bottari [b], Santi Alessandrino [b], Beatrice Carbone [b], Salvatore Adamo [b], Alfio Russo [b], Mariangela Latino [c], Sabrina Conoci [d,e,f], Fortunato Neri [a], Ammar Tariq [a], Carmelo Corsaro [a,*]

[a] *Department of Mathematical and Computer Sciences, Physical Sciences and Earth Sciences (MIFT), University of Messina, Viale F. Stagno D'Alcontres 31, Messina 98166, Italy*
[b] *STMicroelectronics, Stradale Primosole 50, 95125 Catania, Italy*
[c] *CNR-Istituto per i Processi Chimico-Fisici Sede di Messina, V.le F. Stagno d'Alcontres 37, I-98158 Messina, Italy*
[d] *Department of Chemical, Biological, Pharmaceutical and Environmental Sciences (ChiBioFarAm), University of Messina, Viale F. Stagno D'Alcontres 31, Messina 98166, Italy*
[e] *LAB Sense Beyond Nano - URT Department of Sciences Physics and Technologies of Matter (DSFTM) CNR, Viale F. Stagno D'Alcontres 31, Messina 98166, Italy*
[f] *Department of Chemistry "Giacomo Ciamician", University of Bologna, Via Selmi 2, Bologna 40126, Italy*

ARTICLE INFO

Keywords:
GaN power devices
WBG semiconductor
Failure mechanisms
Stress distribution
Raman mapping, SEM

ABSTRACT

The challenge of accurately diagnosing and understanding failure mechanisms in GaN power devices under high-stress conditions has been a persistent issue, particularly with respect to catastrophic failures difficult to detect through conventional electrical measurements. This study focuses on p-GaN-based high-electron-mobility transistors (HEMT) technology device, subjected to high-stress conditions, to analyze the entire device architecture and mainly the structure of the gate–source bridge. SEM analyses reveal significant structural damage, including cracks and voids, particularly near the metal interconnection lines and GaN buffer layers, whereas Raman spectroscopy highlights distortions in the wurtzite GaN crystal structure. By integrating the spectroscopic and morphological results, useful insights into the GaN device layers interested by the failure mechanisms are provided. These data are useful to optimize the multi-layer stacked structures and then to enhance the GaN HEMTs main characteristics.

1. Introduction

Power electronic devices have become indispensable in modern technology, facilitating efficient electrical energy conversion and control across various applications [1]. Over the past century, advancements in power electronics have been driven by significant improvements in device performance, especially in terms of energy conversion efficiency and power density. However, traditional silicon-based devices are now approaching their physical limits, particularly in high-power and high-temperature environments [2]. As a result, the exploration of alternative materials has gained momentum. Gallium Nitride (GaN), a wide bandgap semiconductor stands out for its superior electrical and thermal properties [3,4]. GaN power devices surpass traditional silicon devices by offering higher breakdown voltage, faster switching, and improved thermal conductivity [5]. Since A. Khan et al., pioneering GaN transistor in 1993, the technology has advanced quickly, leading to the commercial release of GaN products by companies like International Rectifier and Efficient Power Conversion [6].

Today, GaN-on-Si devices are widely used in applications such as automotive systems, data centers and communication systems, where their high efficiency and compact form factor are critical [7]. These advancements position GaN as a key material in the future of power electronics, particularly for applications requiring high-speed switching and reduced power loss. GaN is a material which enables a range of new high-frequency topologies; commercial devices now have blocking voltage ranging from 40 V to 1200 V. Generational improvements are driving R_{DS}(ON) and device capacitances lower (R_{DS}(ON) scales approximately as $(L_{GD})^2$ for high voltage devices), but still far from a theoretical limit, and drain-drift length is still 5× larger than the limit for 650 V devices, which means a 10× improvement in transistor area

* Corresponding author.
E-mail address: ccorsaro@unime.it (C. Corsaro).

https://doi.org/10.1016/j.microrel.2025.115754
Received 27 January 2025; Received in revised form 16 March 2025; Accepted 16 April 2025
Available online 23 April 2025
0026-2714/© 2025 The Authors. Published by Elsevier Ltd. This is an open access article under the CC BY-NC-ND license (http://creativecommons.org/licenses/by-nc-nd/4.0/).

for a specific resistance value. For example, the power ICs based on GaN may be applied in high-power, multi-kW applications, with one example being a 3.2 kW, 1 MHz, AC-48 V converter prototype with 65 W/in^3 power density [8]. However, despite their impressive performance, GaN power devices show significant challenges in terms of reliability. A primary limitation is their susceptibility to failure under high electrical and thermal stress [9,10]. Prolonged exposure to such conditions can induce structural degradation, which reduces the operational lifespan of these devices. Defects such as dislocations and point defects, often introduced during epitaxial growth and fabrication, affects significantly the device architecture degradation, leading to failure. Actually, the surface defects can significantly impact carrier lifetime and mobility, while interface defects at the semiconductor-metal/oxide junctions can alter the Schottky barrier height [11,12]. Therefore, the understanding of these degradation mechanisms is crucial to improve the long-term reliability of GaN power devices and ensure their adoption in high-performance applications [13].

To address these challenges, advanced failure analysis techniques are required to uncover the specific mechanisms responsible for device degradation. Among them, Scanning Electron Microscopy (SEM), provides detailed insights into the morphological changes that occur within GaN devices under high-stress conditions [14–17]. Although morphological characterizations allow to highlight the damage, they do not identify and explain its origin. On the contrary, spectroscopic techniques, such as the Raman spectroscopy, allow the identification of structural defects and degradation pathways, offering valuable information for enhancing device design and material processing approaches. Several studies have highlighted the role of hot electrons in accelerating performance degradation, particularly in the on-state medium-term reliability of GaN HEMTs. This mechanism is significant as it shows that temperature has a negligible effect on the degradation process. Different failure mechanisms have been identified, including gate degradation under reverse bias conditions, which can be influenced by initial device defects. Additionally, metal electrode melting has been observed in devices operating at high power and frequency conditions. Parasitic effects such as the kink effect and current collapse are significant issues affecting GaN HEMTs. Again, these effects can be correlated with specific material properties and defects, such as iron doping in the buffer layer [18]. Specifically, electromigration can cause the formation of dark spots in GaN devices, attributed to current filamentation. The lattice mismatch and thermal expansion differences between GaN and common substrates like silicon can lead to high dislocation densities, which might exacerbate electromigration effects. The design of GaN devices, such as the use of step-graded buffers and AlN nucleation layers, helps mitigate strain and dislocations, potentially reducing electromigration risks. GaN HEMTs operate by utilizing a two-dimensional electron gas (2DEG) at the AlGaN/GaN interface. While electromigration is a concern, the specific architecture and operation mode of HEMTs may reduce its impact compared to other semiconductor devices. Instead, thermo-migration in GaN devices, particularly in HEMTs, is a critical issue due to the high-power density and resulting thermal effects. GaN HEMTs are prone to self-heating due to their high-power density, which can elevate the channel temperature significantly [19]. Effective thermal management is crucial for maintaining the performance and reliability of GaN devices. This involves understanding and optimizing heat transfer mechanisms such as conduction, convection, and radiation. On the overall, high temperatures can cause material degradation, including intermixing of metals at interfaces (e.g., Ni/Au near the gate/AlGaN interface) and lattice expansion, which affects device structure and electrical properties: the exposure to high temperatures can significantly increase leakage currents in GaN devices, impacting their electrical performance. Thus, optimizing thermal design by using appropriate packaging (e.g., Flip Chip with Cu pillars) and cooling methods can help manage temperature increases [20]. In addition, further research is needed to enhance the material quality. For this purpose, comprehensive reliability testing, also under various operating conditions, is essential for ensuring long-term stability.

In this paper, micro-Raman mapping and SEM analyses on a multilayer architecture of GaN HEMT subjected to a high-voltage stress are presented and discussed. SEM provides nanoscale resolution (down to ~10 nm) for imaging surface morphology and topography, far surpassing the spatial resolution of standalone Raman spectroscopy (~200 nm for confocal Raman imaging). This enables precise localization of features before chemical analysis with Raman spectroscopy. In fact, Raman spectroscopy offers molecular-level chemical sensitivity by detecting vibrational fingerprints of molecules. It can identify chemical compounds, crystallinity, stress/strain states, and spatial distribution of components and temperature effects. Combining SEM with Raman allows simultaneous structural and chemical analysis, which is not possible with SEM alone. Furthermore, both SEM and Raman are non-destructive techniques, making the combination ideal for analyzing sensitive samples without altering their structure or composition. Both techniques require little to no sample preparation, unlike traditional methods such as XRD or TEM, which may involve extensive sample thinning or staining. The key innovation of this study is the development of a new protocol for device characterization after assembly. This protocol integrates the data obtained from both morphological and spectroscopic analyses to deliver a complete assessment of the device's performance and reliability. By applying this integrated methodology, the study seeks to uncover the specific degradation mechanisms of GaN power devices. In future, this approach could be applied during the fabrication processes for the in-time detection of the device and eventually real-time corrections.

2. Sample and characterization techniques

We analyze failed GaN devices provided by STMicroelectronics (Catania, Italy) of type 650-V p-GaN gate HEMT in PFLAT 5 × 6, after exposure to specific stress conditions. Details are reported in Table 1. We clarify that generally this device starts to degrade and then fails by exhibiting abnormal junction/dielectric leakages, such as on gate to drain, gate to source or drain to source when voltage is applied on those terminals. In our case, it is related to high voltage applied on Drain respect to Source with the Gate to Source shorted and at 0 V: this test is called High Temperature Reverse Bias (HTRB). To assess the reliability of the device and being able to predict the Failure In Time (FIT) for a given mission profile, it is critical to identify the failure mechanisms, the "involved" stressors and to select the potential "fatigue" models. In our GaN technology and for the performed HTRB test, the major stressors are the temperature, the voltage, and the time duration, as expected since high temperatures exacerbate material degradation, including nitrogen escape and thermal cavity formation, which contribute to voids and cracks within the GaN structure. Trial reported in this paper is regarding an HTRB stress at 1200 V for 10 h at 140 °C with a smooth temperature ramp. Temperature control is performed by 4 temperature probes positioned inside the chamber. Through retroactive feedback, the probes thermally stabilize the chamber by balancing the heating provided by the resistors and the cooling provided by a heat transfer liquid. A total of

Table 1
details about the investigated samples.

Technology	V_{DS}	$R_{DS\ (ON)}$ max	I_D	Stress condition	Electrical Characteristics	What observed
p-GaN gate HEMT	650 V	120 mΩ	15 A	HTRB 1200 V 140 °C	Short all pins	Extended burn in active area with FIB cut for SEM analysis and Raman mapping

1000 devices have been stressed with the condition above reported and two devices appear failed after stress. The shape parameter (β) > 1 in the Weibull analysis (commonly used to model failure rates during HTRB testing) indicates wear-out failures from prolonged stress conditions. The two failed devices show a burn of about 10 μm in a random position inside active area on which SEM and Raman analyses were carried out.

Scanning Electron Microscopy (SEM) analyses were performed by using a Zeiss electron microscope (Gemini 2 model), operating at an accelerating voltage of 20 kV. SEM apparatus is coupled with a Quantax EDX spectrometer to carry out energy dispersive X-ray (EDX) analysis. The EDX detected pear-shaped dimension is about 0.7 mm.

Raman spectra excited with the 532 nm diode laser line were obtained with the XploRA Horiba apparatus, equipped with an Olympus BX40 microscope, a 1800 line/mm grating and a Peltier-cooled charge-coupled device (CCD) sensor as the detector; the elastically scattered radiation was rejected by an edge filter. The laser power at the sample surface is about 10 mW when using the 50× microscope objectives, whereas accumulation times were varied, depending on the signal-to-noise ratio, between 20 and 80 s. The sample stage was moved in 5.5 μm increments over an area of approximately 25 μm × 25 μm; all the spectra shown here were normalized to their own integration times.

3. Results and discussion

3.1. Conventional optical inspection and SEM Analyses

The device has been opened from the backside using a parallel lapping technique. Specifically, frame and preform were removed thanks to mechanical polishing and the procedure was stopped when Si-substrate is completely exposed. At this step, sample has been undergone to a dry etch recipe able to remove Si-substrate without attacking GaN-epitaxial level. The optical inspection of the devices (Fig. 1a,b) revealed burned regions extending across several strips of the device.

Then, an extensive series of cross-section SEM analyses were performed to investigate in detail the morphological changes and the specific regions of the device architecture in which the damage occurred. Focused Ion Beam (FIB) cut has been made in the failed burnt region (Fig. 1c and Fig. 2) to enable the recording of detailed cross-section SEM images. After FIB cut, the sample was positioned within the SEM chamber as shown in Fig. 2c.

Fig. 3 shows cross section SEM images of the entire FIB cut region of the device. The overlaying red rectangle indicates the region of interest.

A reconstructed panoramic view of a portion of this device resulting “failed” from the electrical tests (after stress) was carried out (Fig. 4). From a first inspection, the damaged regions are mainly near the connecting path of the metal lines and near the GaN EPI buffer.

To better understand the results, the device architecture is schematically illustrated alongside a high-resolution SEM image of an unaffected device (Fig. 5). The main components of the device, such as the metal lines, GaN buffer, and passivation layers, are clearly identified.

SEM cross-section images, shown in Fig. 6 and comparing unaffected and damaged regions of the device, revealed severe cracks located below the metal drain/gate/source sections in the failed areas.

Specifically, the cracks originated near the drain-side gate edge, extending toward the source. This is attributed to the high electric field at the drain-side gate edge, which generated significant thermal stress that, in turn, triggered the formation of cracks and voids in the GaN structure compromising the device's integrity [21]. Further examination of the device revealed additional damage within the passivation layer, as shown in Fig. 7. The failure extended into this layer, leading to internal strain and delamination. Specifically, cracks in the passivation material were closely associated with the failure signatures observed in the metal interconnects and redistribution layers (RDL) [22]. SEM analysis revealed four key failure signatures, as illustrated in Fig. 7. The first was metal melt damage, primarily located in the Electrostatic Discharge (ESD) protection circuitry. This damage is indicative of excessive current flow, which led to localized melting of the metal contacts, as shown in Region A [23]. The second failure signature was the presence of cracks in the passivation and dielectric layers. These cracks were associated with significant internal strain, as highlighted in Region B [24]. A short circuit between the gate and the field plate of the internal device was also observed, contributing to the device's overall failure, as seen in Region C. Lastly, contact spiking and metal burnout were detected in the metal layers, where the combination of high current density and thermal stress resulted in rapid degradation, as identified in Region D [25]. These findings collectively offer insight into the mechanisms leading to the device's failure.

The failures observed were largely driven by the design and performance of the RDL structure, which plays a crucial role in routing signals across the device. The RDL consists of multiple layers of metal interconnections, insulating materials, and vias, providing signal routing and thermal management. However, the RDL structure exhibited significant deformation under high current densities. As reported in literature [26] polyimide has relatively low thermal conductivity, so it can hinder effective heat dissipation. When encapsulated, the heat generated within GaN devices, which are known for high power density and thermal output, may not transfer efficiently through the polyimide layer, leading to localized overheating in the areas directly beneath the encapsulation [27]. It is already known that the encapsulation layer can create significant temperature gradients within the device. If the thermal conductivity of the encapsulating polymer is low, it can cause heat to accumulate at the interface between the RDL and the polyimide, potentially leading to more severe burning in that area. Conversely, if heat is not effectively dissipated from the center of the GaN device, it may also suffer from overheating, but this would depend on how well heat can spread through the device structure itself. Hence, according to SEM evidence, the failure mechanism was primarily driven by thermo-migration, where a temperature gradient caused material to migrate from the center of the RDL (poor heat dissipation) to the edges (better heat dissipation). This redistribution of material resulted in voids and deformation, leading to open-circuit breakage in the RDL. The electromigration flux was also considered, but the SEM results suggest that thermo-migration, rather than electromigration, was the dominant process responsible for material displacement and eventual failure. The

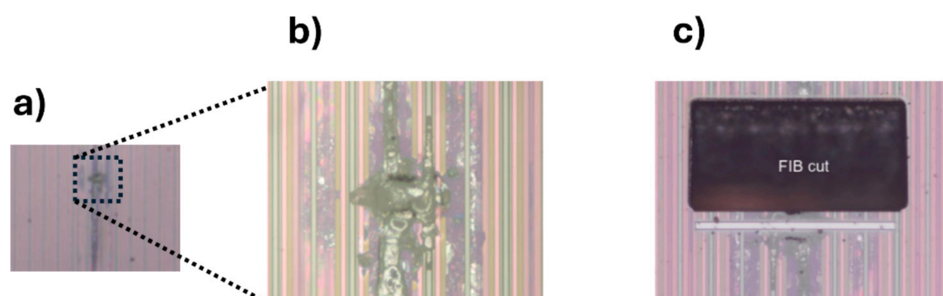

Fig. 1. Optical images of the sample at 10× (a), 50× of magnification before (b) and after (c) FIB cross-sectioning.

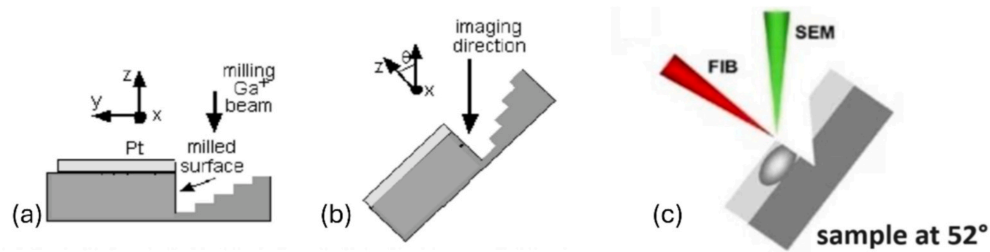

Fig. 2. Operative configuration adopted to acquire SEM images in cross and the FIB working procedure.

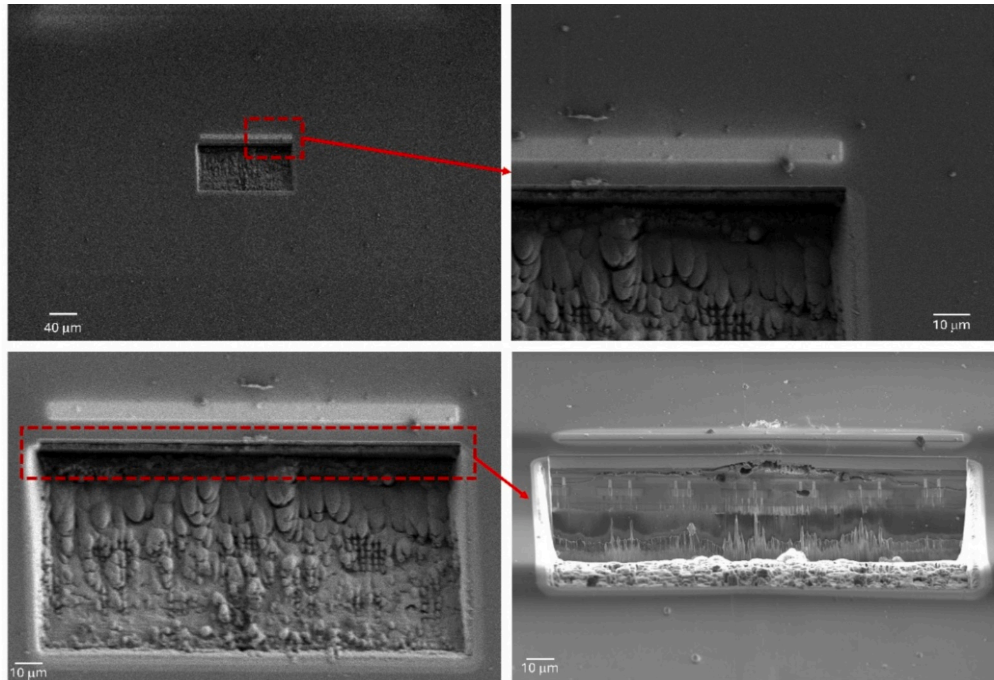

Fig. 3. Cross section SEM image of the entire FIB cut region of the device. In red the region of interest to be investigated.

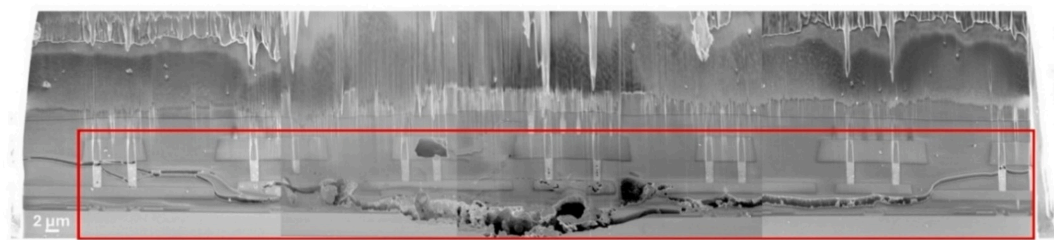

Fig. 4. A panoramic SEM image of a portion of the "failed" device.

Joule heating effect exacerbated the device failure by causing further delamination between the RDL and the PI dielectric layer (Fig. 7). High temperatures generated during device operation led to thermal expansion and mechanical stress, resulting in the detachment of the RDL from the underlying passivation layers. This delamination further contributed to electrical failure, as it disrupted the continuity of the metal interconnections [28].

SEM images show that craters and cracks are concentrated in high-stress regions, at depths of 15–35 μm, predominantly observed near gate and drain regions where electric fields are highest, whereas breakdown paths align along high-current regions between electrodes. To evaluate the elemental composition of the analyzed devices, a quantitative analysis of the energy dispersive X-ray spectroscopy (EDS) spectra was performed using an accelerating voltage of 14 kV. In Fig. 8 are shown EDS microanalyses of device architecture in damaged and unaffected layer regions. The EDS spectrum obviously showed the presence of Ga, Al and N elements together with those of some metal species (W, Ti etc.) assigned to DEG and contact ohmic parts. As shown in GaN device architecture (Fig. 5) and SEM images, the source and drain electrodes pierce through the top AlGaN layer to form an ohmic contact with the underlying 2DEG. This creates a short- circuit between the source and the drain until the 2DEG "pool" of electrons is depleted and the semi-insulating GaN crystal can block the flow of current.

By comparing the unaffected and failed devices, it emerges that the EDS estimated Ga/N ratio is higher than 7 and lower than 2 for the unaffected and damaged sites, respectively. It seems that the amount of

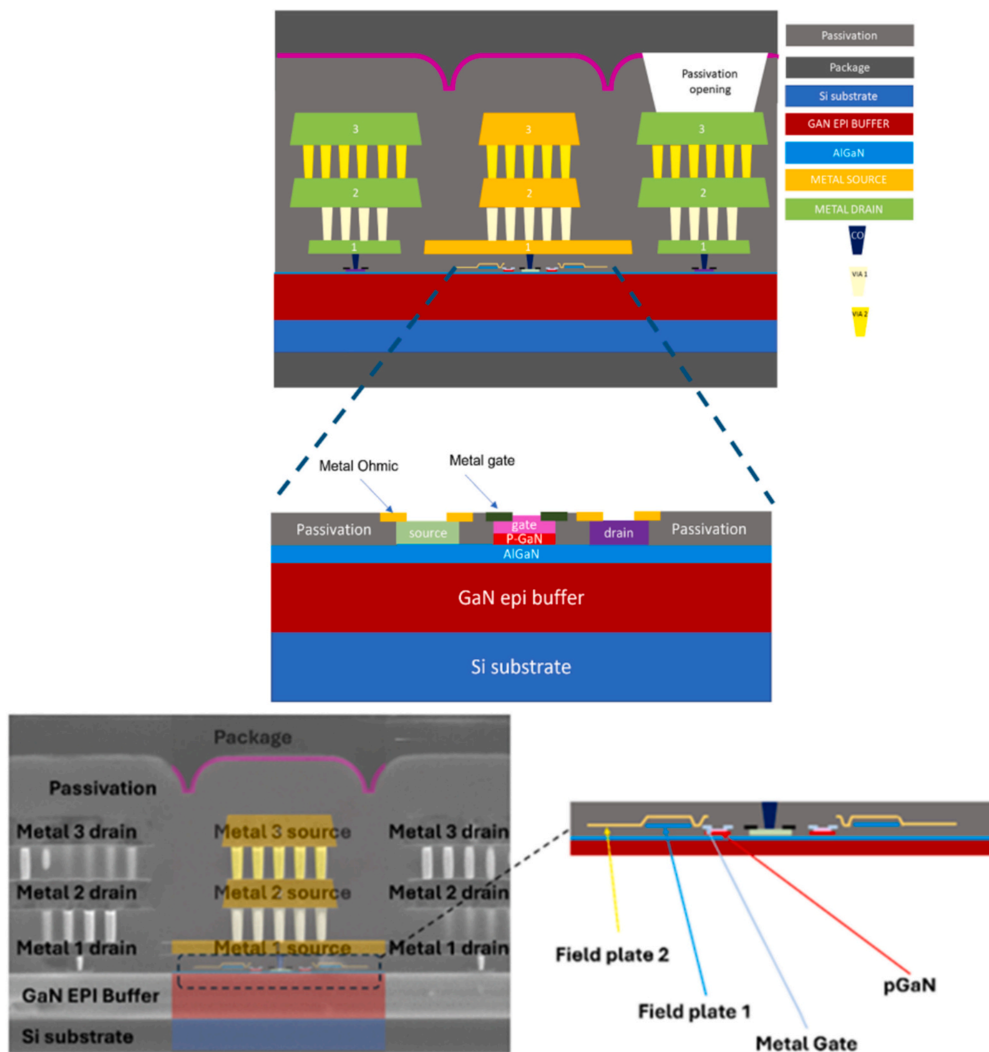

Fig. 5. GaN device architecture and their main components (top panel); SEM image at high resolution (bottom panel) in an unaffected region and corresponding details.

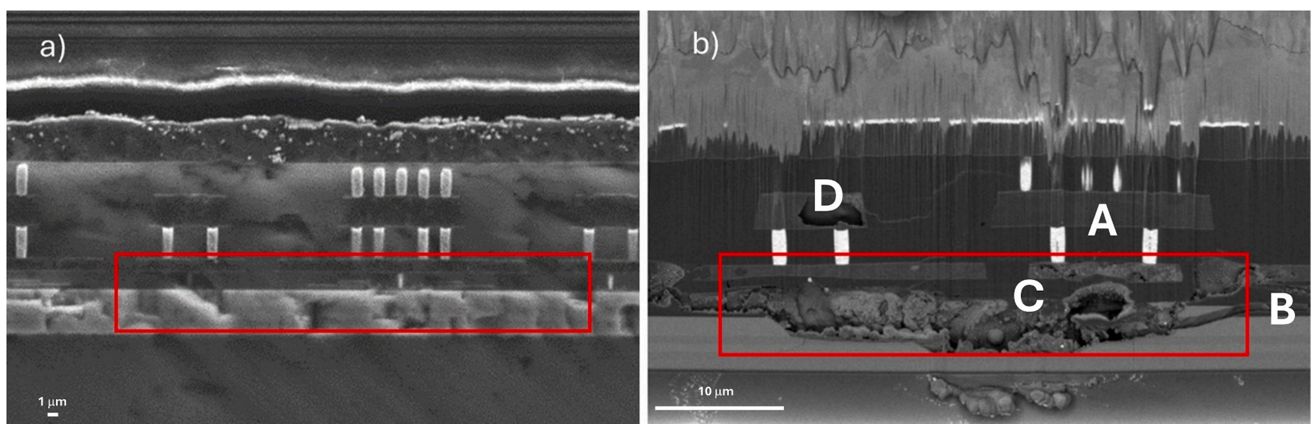

Fig. 6. SEM images on FIB cross section of the device in (a) unaffected and (b) failed regions with red rectangles identify the region where the drain, gate and source are located. For the details of regions A, B, C and D see text and Fig. 7.

gallium with respect to nitrogen decreases. In addition, in some damaged regions, nitrogen was not detected, or its content is very low as well as the oxygen and titanium content increases, indicating that the underlying substrate is exposed. Specifically, EDS analyses show that the peak of the N element can be seen in the GaN area outside the channel and, in the damaged regions, the GaN stoichiometric ratio is not perfectly respected. Voids formed due to nitrogen escape during high electric field stress are typically sub-micrometer to several micrometers

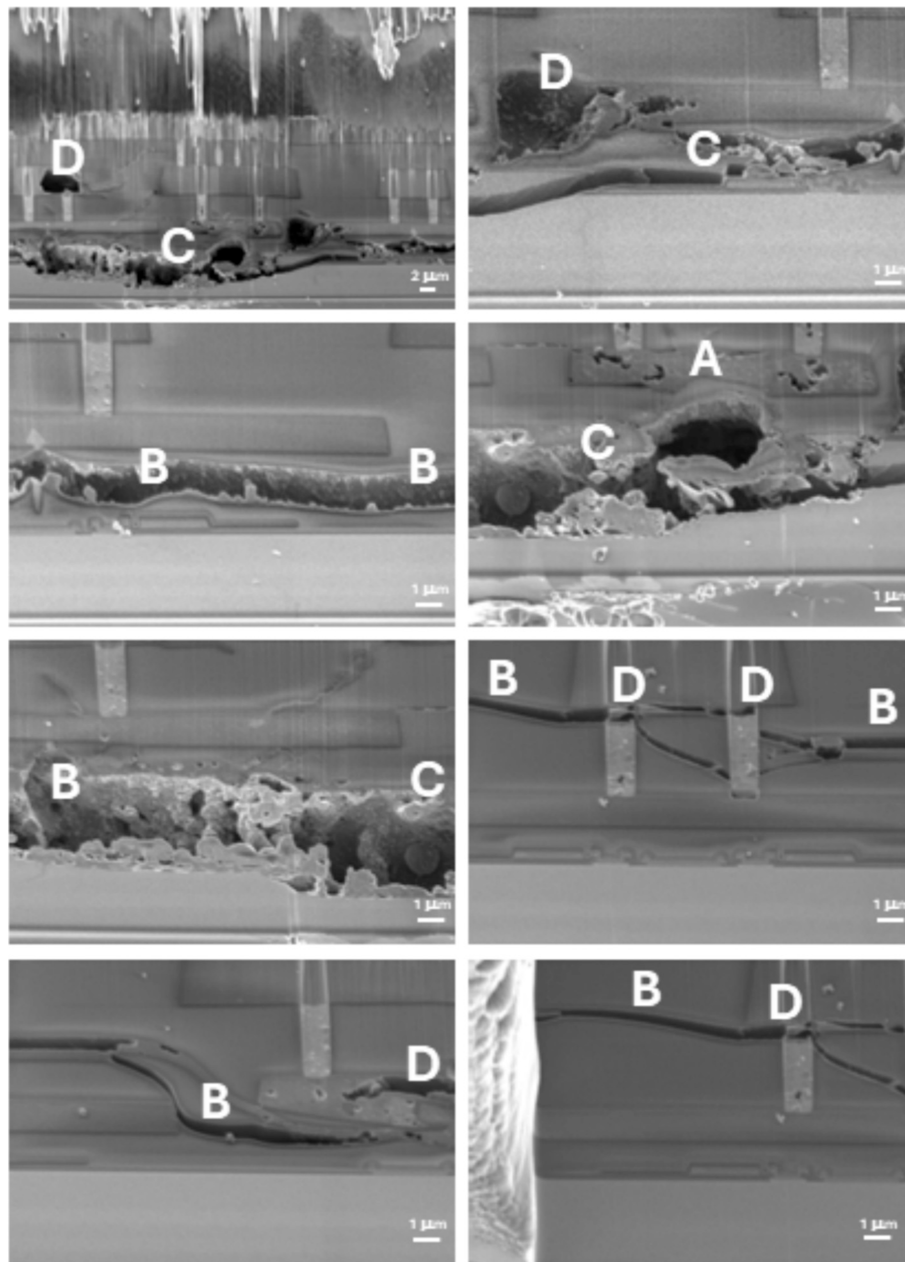

Fig. 7. HR SEM images of the device above the metal contact sections and in the passivation region. Letters indicate the observed failure signatures described in the text.

in size. These voids are also near breakdown regions where thermal and electrical stress is highest as reported in Ref. [29]. It can be assumed that under stress, defects and damage on the surface of the GaN material will form a leakage path, such as nitrogen vacancy-related shallow donors. The current density in the leakage path is very high, which results in a lot of heat. Therefore, when the temperature is high enough to decompose GaN, the N element escapes from the surface, and the Ga element is left in the leakage path, connecting the two electrodes together.

3.2. Raman Analysis

Fig. 9 shows representative Raman spectra of the failed device subjected to 1200 V at 140 °C. These spectra were recorded after the silicon substrate was removed and data were collected from both "unaffected" (position 1) and "damaged" (positions 2 to 5) regions.

In a few surface points, a Si TO mode signal at 521 cm^{-1} was detected, suggesting that some remnants of the silicon substrate were still present [30]. The spectra also revealed characteristic GaN phonon modes, particularly the E_2(high) mode at about 570 cm^{-1}, which is associated with atomic oscillations along the c-plane of GaN's wurtzite structure. This mode is sensitive to lattice strain elongations and is a key marker for detecting residual stress in GaN HEMT devices throughout the AlGaN/GaN heterostructure. Additionally, the A_1 longitudinal optical (LO) mode at 470 cm^{-1} was observed, which undergoes nearly elastic scattering through collisions with hot electrons in GaN HEMT channels. These collisions reduce the lifetime of LO phonons, as reported in the literature [31]. Subsequent Raman mapping was performed in the FIB cut region (154.1 µm × 84.58 µm) of the same device to further investigate the Raman changes at different architecture levels, such as the epitaxial layer. The Raman signal was collected from the entire device structure, as illustrated in Fig. 10.

To make the process followed even clearer, Fig. 11 provides a

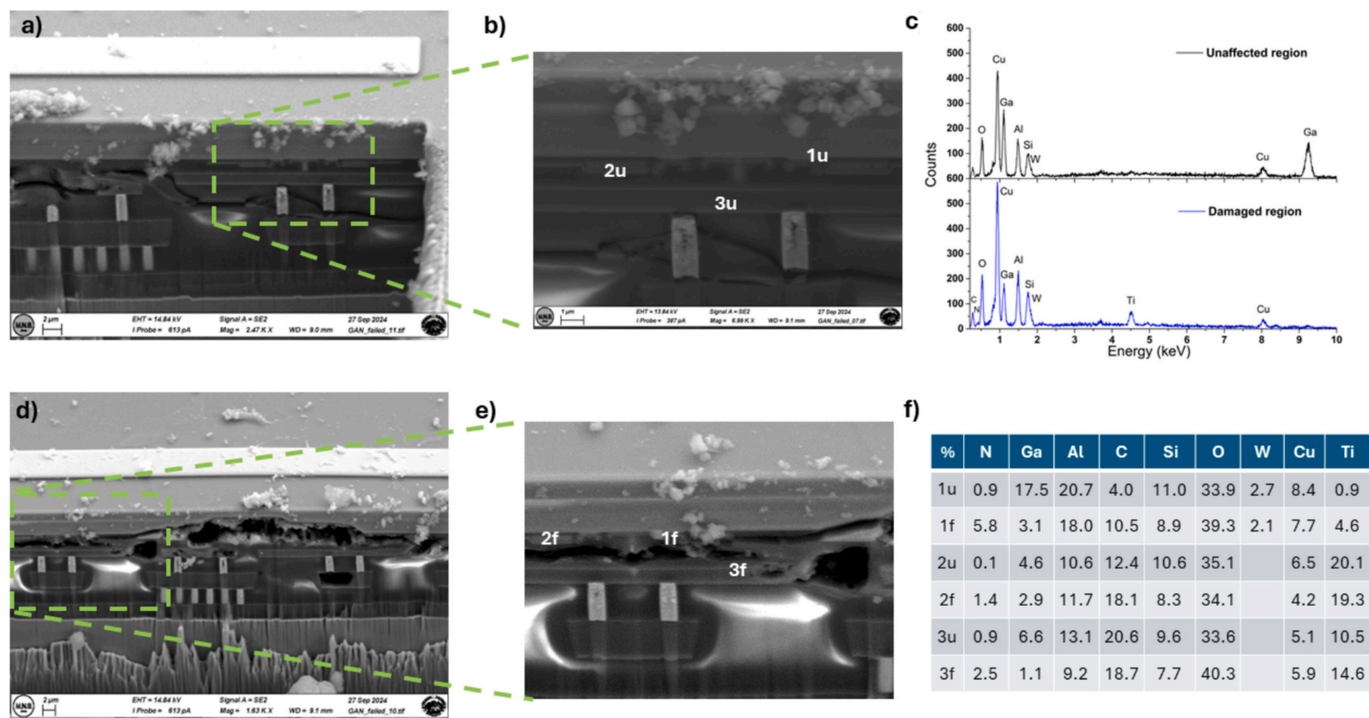

%	N	Ga	Al	C	Si	O	W	Cu	Ti
1u	0.9	17.5	20.7	4.0	11.0	33.9	2.7	8.4	0.9
1f	5.8	3.1	18.0	10.5	8.9	39.3	2.1	7.7	4.6
2u	0.1	4.6	10.6	12.4	10.6	35.1		6.5	20.1
2f	1.4	2.9	11.7	18.1	8.3	34.1		4.2	19.3
3u	0.9	6.6	13.1	20.6	9.6	33.6		5.1	10.5
3f	2.5	1.1	9.2	18.7	7.7	40.3		5.9	14.6

Fig. 8. SEM analysis on unaffected (a,b) and damaged regions (d,e) of the analyzed device; representative EDS spectra (c) and elemental composition (f) evaluated in the highlighted points.

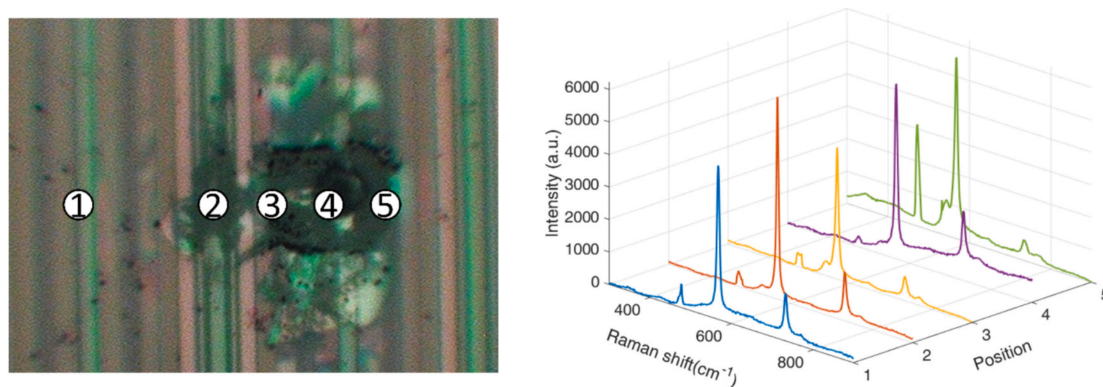

Fig. 9. Representative Raman spectra of failed device after HTRB 1200 V 140 °C.

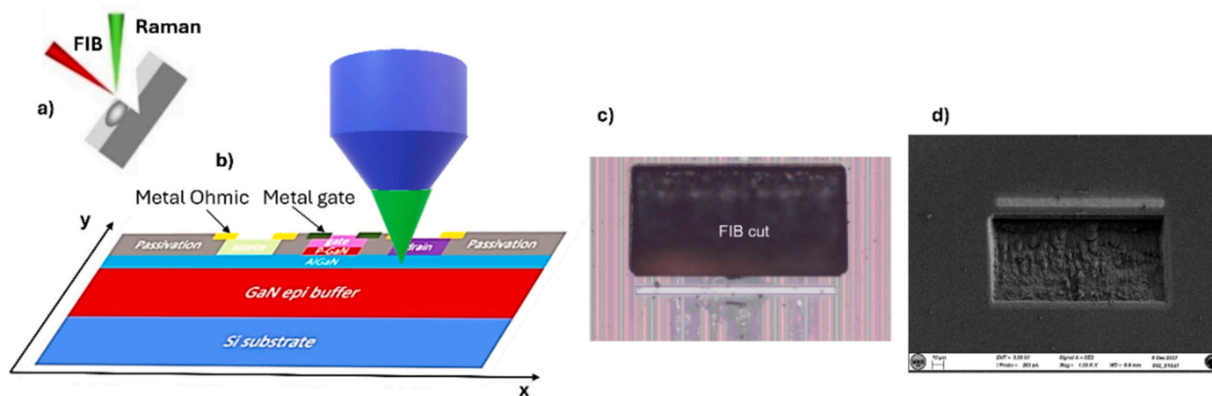

Fig. 10. (a) Operative configuration adopted to acquire Raman spectra in cross, (b) for probing the different layers of the device architecture, (c) FIB cut region made in the failed region, and (d) SEM image of the FIB region.

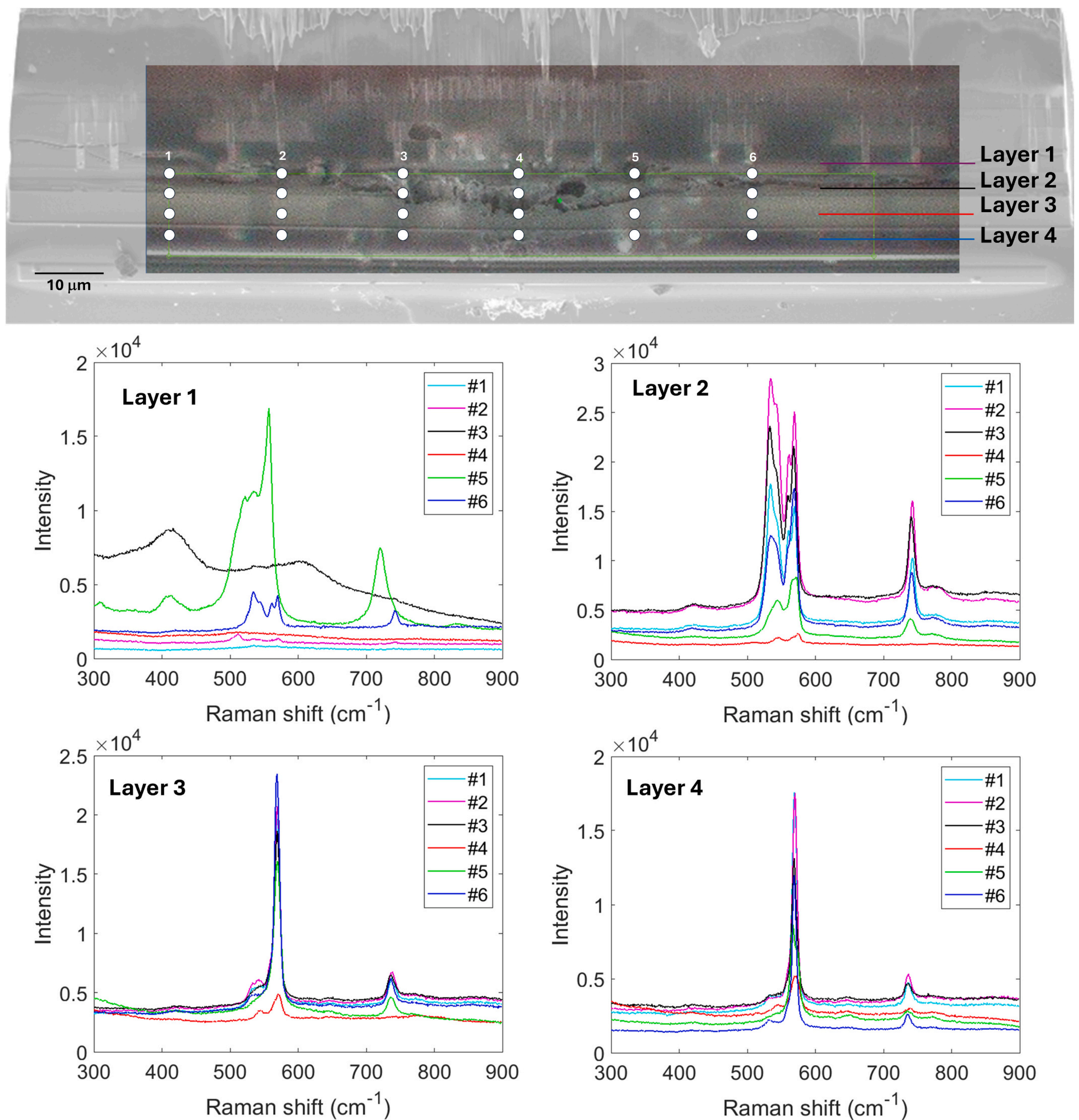

Fig. 11. Panoramic SEM image of the "failed" device, superimposed to the optical image in which the Raman mapping data were acquired (top panel), and the Raman data coming from the different layers and in different point along each layer in order to investigate both the unaffected and damaged regions (bottom panels).

panoramic SEM image of the failed device superimposed onto the optical image, showing the locations where Raman mapping data were obtained. Raman spectra from the GaN buffer layers (layers 3 and 4) predominantly displayed the E_2(high) and A_1(LO) vibrational modes, centered at about 568 and 737 cm^{-1}, respectively (Fig. 11 bottom panels). Interestingly, the intensity of A_1(TO) and E_1(TO) bands from the AlGaN/GaN heterostructure, centered at 534 and 561 cm^{-1} respectively, was significantly lower with respect to the other layers [31]. The observed changes are ascribed to the induced effects of an inhomogeneous electric field distribution, which determines the cracks/fails coming from the epitaxy layer. These changes are clearly observed from SEM images but are also indirectly evidenced by Raman vibrational mode modifications and in good agreement with HTRB tests. We outline this concept in view of the fact that the Raman technique (apparently less intuitive) could be used routinely to detect device structural defects and in turn their damaged regions, even before more expensive tests are performed. In the future, an automated protocol for Raman data analysis could be developed for a large scale application.

To this purpose, the trends discussed below are more interesting. As shown in Fig. 12, the E_2(high)/A_1(LO) ratio exceeded the value of 3 in the GaN buffer layers, but in the damaged regions (positions 3 to 5), this ratio dropped to 1.5, indicating a deformation of the hexagonal wurtzite

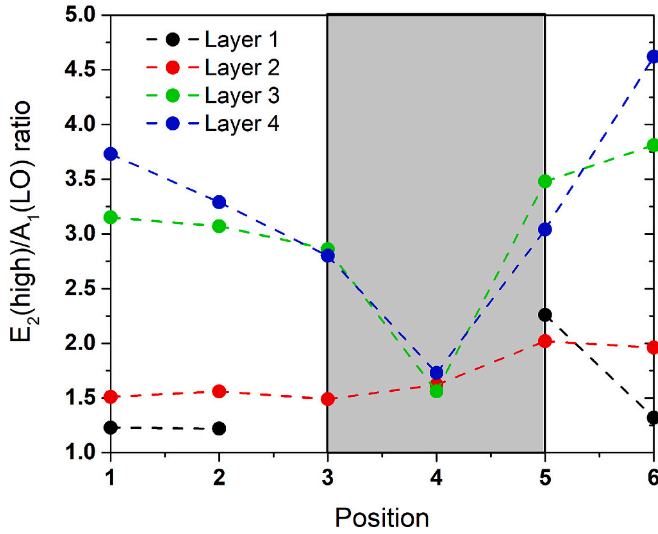

Fig. 12. E_2(high)/A_1(LO) ratio for all the considered layers at the different positions. Positions 3 and 4 of layer 1, due to the device damage, show a completely altered spectrum (see Fig. 11) not allowing a deconvolution.

GaN structure, which is associated with reduced free-electron densities due to the absence of n-type dopants [32]. Further, at the device epitaxial layer (layer 2), the E_2(high)/A_1(LO) ratio remained below 2, although a slight increase was observed near the damaged regions (positions 3 to 5). This is noteworthy because the A_1(LO) mode varies with carrier density due to strong coupling with plasmons and its polar nature, whereas the E_2(high) mode is typically used to probe biaxial stress in GaN due to its non-polar behavior [33,34]. These observations suggest that the high electric field, and the consequent melting, altered the internal structural parameters of wurtzite GaN, beyond the macroscopic strain induced by the short-circuit occurrence. This effect also impacted the doping homogeneity in the GaN drift layer (epilayer), which is essential for high-voltage GaN-based devices.

The decrease in the E_2(high)/A_1(LO) Raman intensity ratio in GaN layers of power devices can indeed reflect changes in carrier density. This relationship is based on the sensitivity of the A_1(LO) mode to free carriers, as it is strongly coupled to plasmon-phonon interactions. A decrease in this ratio indicates an increase in carrier density because the A_1(LO) mode becomes more prominent due to stronger coupling with free carriers. Conversely, a higher ratio suggests lower carrier density or reduced plasmon-phonon coupling. Theoretical models like plasmon-phonon coupling and empirical relationships between Raman intensity ratios and carrier densities provide a robust framework for interpreting changes in E_2(high)/A_1(LO) [35–37]. This coupling modifies the intensity, linewidth, and frequency of the A_1(LO) mode, making it a sensitive indicator of carrier density. The relationship can be described using the dielectric function formalism, where the coupled modes are derived from the longitudinal dielectric response:

$$\epsilon(\omega) = \epsilon_\infty \left(1 - \frac{\omega_L^2}{\omega^2 - i\gamma\omega} - \frac{\omega_p^2}{\omega^2 - i\gamma_p\omega}\right)$$

where ϵ_∞ is the high-frequency dielectric constant, ω_L is the longitudinal optical phonon frequency, $\omega_p = (ne^2/m^*\epsilon_0)^{1/2}$ represents the plasma frequency (depends on carrier density n), and γ_p is the damping constants for phonons and plasmons. As n (carrier density) increases, the plasma frequency (ω_p) shifts, enhancing the Raman intensity of A_1(LO). In detail, the E_2(high) mode is a non-polar phonon mode that is unaffected by free carrier interactions. Its intensity remains relatively constant regardless of carrier density. Thus, changes in the E_2(high)/A_1(LO) ratio directly reflect variations in A_1(LO), which are tied to carrier density. The intensity of A_1(LO) increases with higher n, following plasmon-phonon coupling dynamics. Generally, the decrement of the E_2(high)/A_1(LO) ratio correlates with increasing carrier densities typically ranging from 10^{16} to 10^{19} cm^{-3} [38,39]. Thus, monitoring changes in the E_2(high)/A_1(LO) ratio provides insights into carrier injection, depletion, or trapping under operation, and it helps identify regions with high carrier concentrations that may lead to hotspots or reliability issues. This makes Raman spectroscopy a valuable tool for evaluating and optimizing GaN power devices by providing non-destructive insights into carrier dynamics and material quality. Ultimately, by correlating Raman measurements with electrical performance, manufacturers can optimize doping levels and reduce defects that impact reliability.

Additionally, a systematic trend in Raman shifts and intensities was observed for the vibrational modes in the 500–600 cm^{-1} range, including the E_2(high), E_1(TO), A_1(TO) modes, and an oxygen-induced defect vibrational mode centered at around 544 cm^{-1}. Fig. 13 provides an in-depth analysis of the Raman spectral profiles along the second layer (epitaxial layer) of the device, focusing on both unaffected and damaged regions. In Fig. 13(a), a 3D Raman spectral profile is shown, outlining the spectral differences as one moves from unaffected positions (1, 2, 6) to damaged positions (3, 4, 5). The variations in the Raman spectra are observed in terms of shifts and intensity. Fig. 13(b-d) presents the fitting of these Raman spectra using four Gaussian components within the spectral range of 480–620 cm^{-1}, corresponding to different positions in the device. Fig. 13(b) illustrates the fitting for an unaffected region (position 1), where the Raman spectrum appears more well-defined. In contrast, Fig. 13(c) shows the fitting for a failed region (position 5), where the spectrum is less defined due to the damage. Finally, Fig. 13(d) displays the spectrum from a partially unaffected region (position 6), where the features are intermediate between the unaffected and damaged areas. This analysis reveals that the vibrational modes, especially in the 500–600 cm^{-1} range, exhibit clear shifts between the different regions of the device, indicating structural changes.

Fitting parameters, including Raman shifts and intensity ratios of the GaN vibrational modes, followed well-defined trends (as seen in Fig. 14). In the damaged regions, the GaN material lattice exhibited compression, indicated by the increase in E_1(TO) and E_2(high) Raman shifts, consistent with literature data [40]. Moreover, the E_2(high) mode is commonly used to estimate stress by using the equation $\sigma = \Delta\omega/k_R$ which relates the Raman shift ($\Delta\omega$) in cm^{-1} to the stress (σ) in GPa while k_R is the Raman stress factor which assumes values ranging from −2.69 cm^{-1}/GPa to −2.9 cm^{-1}/GPa for the (0001) plane. In our case, referring to the spectra in the damaged region, $\Delta\omega = 5$ cm^{-1}, k_R is assumed of −2.9 cm^{-1}/GPa then $\sigma = -1.73$ GPa indicating compressive stress [41]. A slight redshift of the GaN:O mode vibrational band was also observed. Furthermore, the A_1(TO) mode, attributed to interface and quasi-confined phonons, showed an opposite trend compared to the E_2(high) mode, providing further evidence of strain in the stressed device (Fig. 14).

The ratios between the intensities of the GaN modes along layer 2 (Fig. 14b) showed that the A_1(TO)/GaN and A_1(TO)/E_2(high) ratios decreased in the damaged region but increased as one moved away from it. Further analysis is needed to clarify these trends, particularly the transitions between different modes, which are correlated with electronic transitions associated with DX-like center behavior of substitutional oxygen on nitrogen sites [42].

4. Conclusion

This study provides valuable insights into the physical failure modes of GaN power devices, based on experimental evidence and detailed analyses carried out by combining SEM imaging (with FIB) and Raman spectroscopy. The investigation reveals critical morphological changes and degradation mechanisms in GaN devices. Observed dark spots on device strips are indicative of thermo-migration, leading to localized damage. These spots are notably present on the grounded contact, underscoring the significant role of both high-power dissipation and

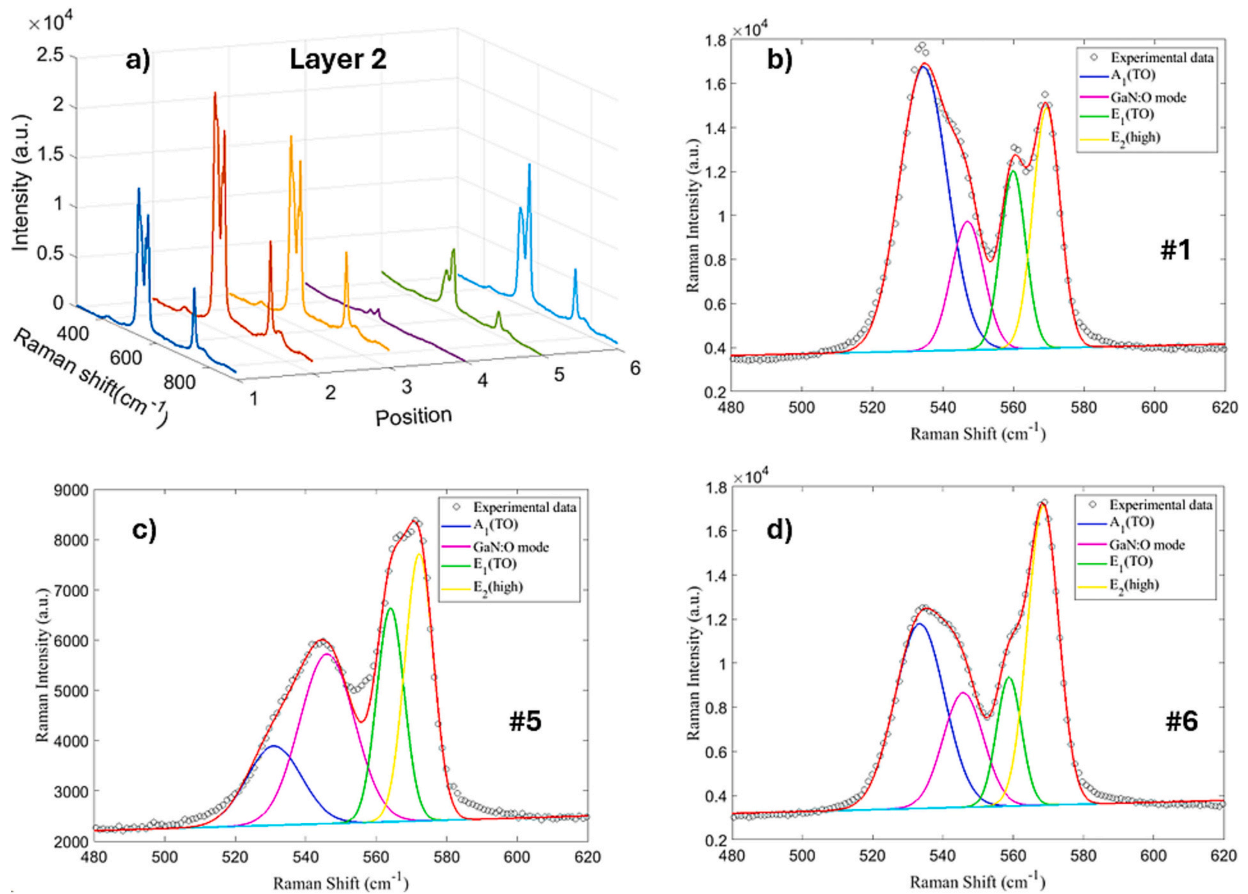

Fig. 13. (a) 3D Raman spectral profiles acquired along the second layer but in different positions and (b-d) Representative fitting profiles with four Gaussian components performed in the spectral region 480–620 cm^{-1}.

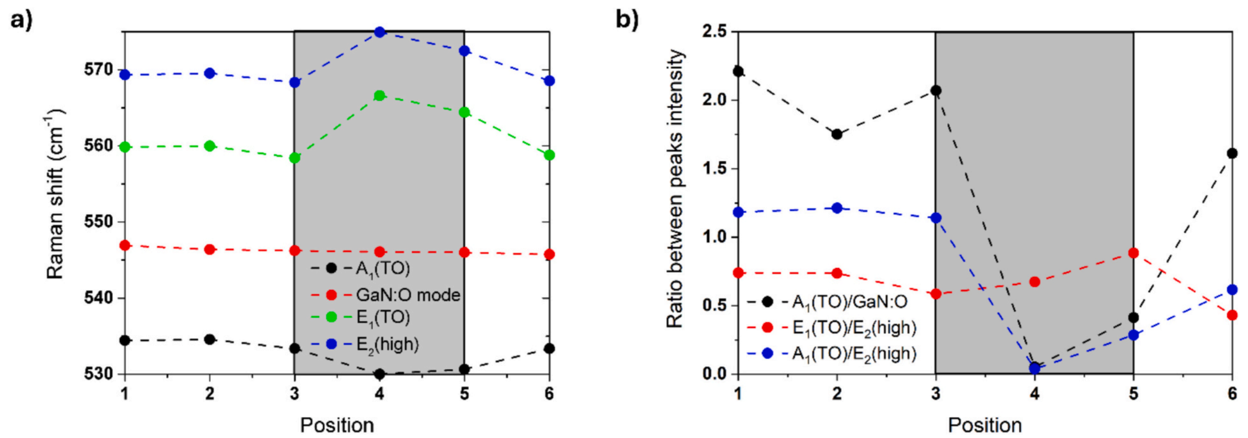

Fig. 14. Raman shifts trend along the layer 2 (a) and ratios between the intensity of GaN modes along the layer 2.

current flow in device degradation. Micro-Raman analyses further highlight distortions in the wurtzite GaN crystal structure, particularly under the source-drain and gate metal regions. This distortion suggests that strain within the GaN chip contributes to the observed failures. The combination of thermal and electrical stresses induces semiconductor melting, leading to catastrophic device failure, as observed by overstressing the device with the high voltage applied. Addressing these issues through improved design and material processing is crucial for enhancing the long-term reliability and efficiency of GaN-based power devices.

In summary, SEM data used to identify surface defects, dislocations, and cracks that can propagate under stress give useful indications to implement improved epitaxial growth techniques (e.g., MOCVD) to reduce threading dislocations and surface roughness, which are common reliability issues in GaN devices. Raman spectroscopy detects residual stress in GaN layers. So, stress could be minimized by optimizing substrate materials and buffer layers (e.g., AlGaN/AlN) in order to reduce strain-induced degradation. Moreover, the development of trap-free dielectrics and interfaces as well as the use of advanced passivation layers could be useful to mitigate charge trapping, which causes current collapse, to stabilize surface states and reduce trapping effects. In addition, in future the integration of protection circuits with GaN

HEMTs could be adopted to handle transient events like power surges or short circuits. The authors, taking into account the experimental data reported in this paper, suggest to use routinely Raman spectroscopy during stress tests to monitor real-time changes in stress or strain within the material. Implementing effective thermal management techniques, such as using micro-trench structures filled with high thermal conductivity materials like copper, can help mitigate thermo-migration by reducing temperature gradients. Improving the design of metal interconnects and using materials with higher electromigration resistance can help mitigate these effects. Additionally, reducing current densities through better device design can also be beneficial as well as implementing efficient cooling systems, such as micro-trench structures or advanced packaging techniques, can reduce temperature gradients and mitigate thermo-migration effects.

CRediT authorship contribution statement

Enza Fazio: Conceptualization, Investigation, Data curation, Writing – review & editing. **Cettina Bottari:** Investigation, Data curation, Writing – review & editing. **Santi Alessandrino:** Investigation, Writing – review & editing. **Beatrice Carbone:** Methodology, Writing – review & editing. **Salvatore Adamo:** Methodology, Writing – review & editing. **Alfio Russo:** Methodology, Writing – review & editing. **Mariangela Latino:** Investigation, Writing – review & editing. **Sabrina Conoci:** Supervision, Writing – review & editing. **Fortunato Neri:** Supervision, Writing – review & editing. **Ammar Tariq:** Investigation, Writing – review & editing. **Carmelo Corsaro:** Visualization, Investigation, Writing – review & editing.

Declaration of competing interest

The authors declare the following financial interests/personal relationships which may be considered as potential competing interests: Authors Cettina Bottari, Santi Alessandrino, Beatrice Carbone, Salvatore Adamo and Alfio Russo were employed by the company ST Microelectronics. The remaining authors declare that they have no known competing financial interests or personal relationships that could have appeared to influence the work reported in this paper.

Acknowledgments

This work has been carried out in the framework of the European Project GaN4AP (Gallium Nitride for Advanced Power Applications). The project has received funding from the Electronic Component Systems for European Leadership Joint Undertaking (ECSELJU) under grant agreement no. 101007310. This Joint Undertaking received support from the European Union's Horizon 2020 research and innovation programme, and Italy, Germany, France, Poland, Czech Republic, and the Netherlands.

Data availability

The data that has been used is confidential.

References

[1] A. Chakraborty, Advancements in power electronics and drives in interface with growing renewable energy resources, Renew. Sust. Energ. Rev. 15 (4) (2011) 1816–1827, https://doi.org/10.1016/j.rser.2010.12.005.

[2] Y. Zhong, J. Zhang, S. Wu, L. Jia, X. Yang, Y. Liu, Q. Sun, A review on the GaN-on-Si power electronic devices, Fundam. Res. 2 (3) (2022) 462–475, https://doi.org/10.1016/j.fmre.2021.11.028.

[3] S.M.S.H. Rafin, R. Ahmed, M.A. Haque, M.K. Hossain, M.A. Haque, O. A. Mohammed, Power electronics revolutionized: a comprehensive analysis of emerging wide and Ultrawide bandgap devices, Micromachines 14 (2023) 2045, https://doi.org/10.3390/mi14112045.

[4] M. Shur, Wide band gap semiconductor technology: state-of-the-art, Solid State Electron. 155 (2019) 65–75, https://doi.org/10.1016/j.sse.2019.03.020.

[5] E.A. Jones, F.F. Wang, D. Costinett, Review of commercial GaN power devices and GaN-based converter design challenges, IEEE, J. Emerg. Sel. Top. Power Electron. 4 (3) (2016) 707–719, https://doi.org/10.1109/JESTPE.2016.2582685.

[6] M. Asif, J.N. Kuznia, A.R. Bhattarai, D.T. Olson, Metal semiconductor field effect transistor based on single crystal GaN, Appl. Phys. Lett. 62 (15) (1993) 1786–1787, https://doi.org/10.1063/1.109549.

[7] A. Letellier, M.R. Dubois, J.P. Trovao, H. Maher, Gallium nitride semiconductors in power electronics for electric vehicles: advantages and challenges, IEEE (VPPC) 1-6 (2015), https://doi.org/10.1109/VPPC.2015.7352955.

[8] Q. Huang, R. Yu, A. Q. Huang and W. Yu, "Adaptive zero-voltage-switching control and hybrid current control for high efficiency GaN-based MHz Totem-pole PFC rectifier," 2017 IEEE applied power electronics conference and exposition (APEC), Tampa, FL, USA, 2017, pp. 1763–1770, doi: https://doi.org/10.1109/APEC.2017.7930937.

[9] S. Musumeci, V. Barba, Gallium nitride power devices in power electronics applications: state of art and perspectives, Energies 16 (9) (2023) 3894, https://doi.org/10.3390/en16093894.

[10] T.J. Flack, B.N. Pushpakaran, B.S. Bayne, GaN technology for power electronic applications: a review, J. Electron. Mater. 45 (2016) 2673–2682, https://doi.org/10.1007/s11664-016-4435-3.

[11] Y. Song, Z. Lv, J. Bai, S. Niu, Z. Wu, L. Qin, L. Wang, Processes of the reliability and degradation mechanism of high-power semiconductor lasers, Crystals 12 (6) (2022) 765, https://doi.org/10.3390/cryst12060765.

[12] G.G. Njema, J.K. Kibet, S.M. Ngari, A review of interface engineering characteristics for high performance perovskite solar cells, measurement, Energy 2, 100005 (2024), https://doi.org/10.1016/j.meaene.2024.100005.

[13] C. De Santi, et al., Review on the degradation of GaN-based lateral power transistors, e-prime-advances in electrical engineering, Electronics and Energy 1 (2021) 100018, https://doi.org/10.1016/j.prime.2021.100018.

[14] P. Kolmer, A. Shukla, J. Song, Methods of material and surface analysis for the evaluation of failure modes for electrical connectors, Technologies 10 (6) (2022) 124, https://doi.org/10.3390/technologies10060124.

[15] P. Li, S. Chen, H. Dai, Z. Yang, Z. Chen, Y. Wang, H. Duan, Recent advances in focused ion beam nanofabrication for nanostructures and devices: fundamentals and applications, Nanoscale 13 (3) (2020) 1529–1565, https://doi.org/10.1039/D0NR07539F.

[16] K. Kant, D. Losic, Focused ion beam (FIB) Technology for Micro- and Nanoscale Fabrications, in: Z. Wang (Ed.), FIB Nanostructures, Lecture Notes in Nanoscale Science and Technology, vol. 20, Springer, Cham, 2013, https://doi.org/10.1007/978-3-319-02874-3_1.

[17] R.A. Khadar, C. Liu, L. Zhang, P. Xiang, K. Cheng, E. Matioli, 820-V GaN-on-Si quasi-vertical pin diodes with BFOM of 2.0 GW/cm2, IEEE Electron Device Lett. 39 (3) (2018) 401–404, https://doi.org/10.1109/LED.2018.2793669.

[18] G. Meneghesso, C. Dua, M. Peroni, M. Uren, E. Zanoni, Parasitic effects and reliability issues on GaN based HEMTs, Extended Abstracts of the 2007 International Conference on Solid State Devices and Materials, Tsukuba, 2007, pp. 160–161. https://doi.org/10.7567/SSDM.2007.G-2-1.

[19] M. Haziq, S. Falina, A.A. Manaf, H. Kawarada, M. Syamsul, Challenges and opportunities for high-power and high-frequency AlGaN/GaN high-Electron-mobility transistor (HEMT) applications: a review, Micromachines 13 (2022) 2133, https://doi.org/10.3390/mi13122133.

[20] Md Abu Jafar Rasel, D. Zhang, A. Chen, M. Thomas, S.D. House, W. Kuo, J. Watt, A. Islam, N. Glavin, M. Smyth, A. Haque, D.E. Wolfe, S.J. Pearton, Temperature-induced degradation of GaN HEMT: an in situ heating study, J. Vac. Sci. Technol. B 42 (3) (2024) 032209, https://doi.org/10.1116/6.0003490.

[21] X. Cai, C. Du, Z. Sun, R. Ye, H. Liu, Y. Zhang, H. Lu, Recent progress of physical failure analysis of GaN HEMTs, J. Semicond. 42 (5) (2021) 051801, https://doi.org/10.1088/1674-4926/42/5/051801.

[22] J. Lau, et al., Redistribution layers (RDLs) for 2.5 D/3D IC integration, J. Microelectron. Electron. Packag. 11 (1) (2014) 16–24, https://doi.org/10.4071/imaps.406.

[23] J.E. Vinson, J.J. Liou, Electrostatic discharge in semiconductor devices: an overview, Proc. IEEE 86 (2) (1998) 399–420, https://doi.org/10.1109/5.659493.

[24] Daniel Sullivan, Eric Carleton, Failure Analysis, 1st ed., De Gruyter, 2022.

[25] A. Turak, Interfacial degradation in organic optoelectronics, RSC Adv. 3 (18) (2013) 6188–6225, https://doi.org/10.1039/C2RA22770C.

[26] K. Tajiri, *et al.*, Electric field enhancements due to space charge in thin polyimide film, 2019 IEEE Conference on Electrical Insulation and Dielectric Phenomena (CEIDP), Richland, WA, USA, 2019, pp. 781–784, doi: https://doi.org/10.1109/CEIDP47102.2019.9010551.

[27] P. Jongwoon, H. Hyokyun, P. Cheolyoung, Heat transfer property of thin-film encapsulation for OLEDs, Org. Electron. 12 (2011) 227–233, https://doi.org/10.1016/j.orgel.2010.11.023.

[28] P. Nimbalkar, P. Bhaskar, M. Kathaperumal, M. Swaminathan, R.R. Tummala, A review of polymer dielectrics for redistribution layers in interposers and package substrates, Polym 15 (19) (2023) 3895, https://doi.org/10.3390/polym15193895.

[29] P. Peri, K. Fu, H. Fu, Y. Zhao, D.J. Smith, Structural breakdown in high power GaN-on-GaN p-n diode devices stressed to failure, J. Vac. Sci. Technol. A 38 (6) (2020) 063402, https://doi.org/10.1116/6.0000488.

[30] B. Foltyński, MOVPE Growth and Characterization of GaN/InGaN Nanowires and Microrods for Next Generation Solid-State-Lighting Applications, Doctoral dissertation, Dissertation, Rheinisch-Westfälische Technische Hochschule Aachen, 2016. https://publications.rwth-aachen.de/record/672605.

[31] Y. Zeng, J. Ning, J. Zhang, Y. Jia, C. Yan, B. Wang, D. Wang, Raman analysis of E_2 (high) and A_1 (LO) phonon to the stress-free GaN grown on sputtered AlN/

graphene buffer layer, Appl. Sci. 10 (24) (2020) 8814, https://doi.org/10.3390/app10248814.

[32] T. Beechem, A. Christensen, D.S. Green, S. Graham, Assessment of stress contributions in GaN high electron mobility transistors of differing substrates using Raman spectroscopy, J. Appl. Phys. 106 (11) (2009) 114509, https://doi.org/10.1063/1.3267157.

[33] F.A. Ponce, J.W. Steeds, C.D. Dyer, G.D. Pitt, Direct imaging of impurity-induced Raman scattering in GaN, Appl. Phys. Lett. 69 (18) (1996) 2650–2652, https://doi.org/10.1063/1.117547.

[34] A.J.E. N'Dohi, et al., Micro-Raman characterization of homo-epitaxial n doped GaN layers for vertical device applications, AIP Adv. 12 (2) (2022) 025126, https://doi.org/10.1063/5.0082860.

[35] M.A. Ochoa, J.E. Maslar, H.S. Bennett, Extracting electron densities in n-type GaAs from Raman spectra: comparisons with hall measurements, J. Appl. Phys. 128 (7) (2020), https://doi.org/10.1063/5.0011247.

[36] L.H. Robins, E. Horneber, N.A. Sanford, K.A. Bertness, M.D. Brubaker, J. B. Schlager, Raman spectroscopy based measurements of carrier concentration in n-type GaN nanowires grown by plasma-assisted molecular beam epitaxy, J. Appl. Phys. 120 (12) (2016) 124313, https://doi.org/10.1063/1.4963291.

[37] E. Tiras, M. Tanisli, N. Balkan, S. Ardali, E. Iliopoulos, A. Georgakilas, A, determination of the carrier density dependent electron effective mass in InN using infrared and Raman spectra, Phys. Status Solidi B 249 (2012) 1235–1240, https://doi.org/10.1002/pssb.201147500.

[38] T.E.K. Shwe, T. Asaji, R. Kimura, D. Iida, M.A. Najmi, K. Ohkawa, Y. Ishitani, Photoluminescence emission efficiency analysis methodology by integrating Raman spectroscopy of the A1(LO) and E2(high) phonons in a GaInN/GaN Heterostructure, Phys. Status Solidi B 261 (2024) 2400057, https://doi.org/10.1002/pssb.202400057.

[39] L. Li, S. Zhu, L. Cheng, H. Qi, Y. Fan, W. Zheng, Probing carrier concentration of doped GaN single crystals from LO phonon-plasmon coupled modes, JOL 251 (2022) 119214, https://doi.org/10.1016/j.jlumin.2022.119214.

[40] Z. Dahrouch, G. Malta, M. d'Ambrosio, A.A. Messina, M. Musolino, A. Sitta, M. Calabretta, S. Patanè, Assessing the stress induced by novel packaging in GaN HEMT devices via Raman spectroscopy, Appl. Sci. 14 (10) (2024) 4230, https://doi.org/10.3390/app14104230.

[41] B. Han, M. Sun, Y. Chang, S. He, Y. Zhao, C. Qu, W. Qiu, Raman characterization of the in-plane stress tensor of gallium nitride, Materials 16 (2023) 2255, https://doi.org/10.3390/ma16062255.

[42] C. Wetzel, H. Amano, I. Akasaki, J.W. Ager III, J. Grzegory, M. Topf, B.K. Meyer, Localized vibrational modes in GaN : O tracing the formation of oxygen DX-like centers under hydrostatic pressure, Phys. Rev. B 61 (2000) 8202–8206, https://doi.org/10.1103/PhysRevB.61.8202.